

## Research Article

# DSMC Simulation and Experimental Validation of Shock Interaction in Hypersonic Low Density Flow

**Hong Xiao, Yuhe Shang, and Di Wu**

*School of Power and Energy, Northwestern Polytechnical University, Xi'an, Shaanxi 710072, China*

Correspondence should be addressed to Hong Xiao; [xhong@nwpu.edu.cn](mailto:xhong@nwpu.edu.cn)

Received 6 August 2013; Accepted 11 October 2013; Published 30 January 2014

Academic Editors: G. Liang and S. Longo

Copyright © 2014 Hong Xiao et al. This is an open access article distributed under the Creative Commons Attribution License, which permits unrestricted use, distribution, and reproduction in any medium, provided the original work is properly cited.

Direct simulation Monte Carlo (DSMC) of shock interaction in hypersonic low density flow is developed. Three collision molecular models, including hard sphere (HS), variable hard sphere (VHS), and variable soft sphere (VSS), are employed in the DSMC study. The simulations of double-cone and Edney's type IV hypersonic shock interactions in low density flow are performed. Comparisons between DSMC and experimental data are conducted. Investigation of the double-cone hypersonic flow shows that three collision molecular models can predict the trend of pressure coefficient and the Stanton number. HS model shows the best agreement between DSMC simulation and experiment among three collision molecular models. Also, it shows that the agreement between DSMC and experiment is generally good for HS and VHS models in Edney's type IV shock interaction. However, it fails in the VSS model. Both double-cone and Edney's type IV shock interaction simulations show that the DSMC errors depend on the Knudsen number and the models employed for intermolecular interaction. With the increase in the Knudsen number, the DSMC error is decreased. The error is the smallest in HS compared with those in the VHS and VSS models. When the Knudsen number is in the level of  $10^{-4}$ , the DSMC errors, for pressure coefficient, the Stanton number, and the scale of interaction region, are controlled within 10%.

## 1. Introduction

Shock interactions play an important role in hypersonic flows. In the past decade, significant efforts in computational fluid dynamics (CFD) have been exerted to develop prediction techniques for simulating these complex flow structures [1–3]. Most of these works were simulated using the continuum transport equations (Navier-Stokes), which describe the transport of mass, momentum, and energy. These equations are based on the hypothesis that the mean free-path length  $\lambda$  of gas molecules is very small compared with the characteristic dimension  $L$  of the flow. This characteristic dimension can be defined by the flowing gradient length scale

$$L = \frac{\phi}{(\partial\phi/\partial x)}. \quad (1)$$

Here,  $\phi$  is the flow property and it can be density or pressure and so on. Also, the Knudsen number  $Kn$  is usually used to describe low density flow:

$$Kn = \frac{\lambda}{L}. \quad (2)$$

Flows with  $Kn > 10$  are called “free molecular flows.” In this regime, intermolecular collisions rarely occur, and the flow is completely dominated by the interaction between the gas and the wall. Flows in the free molecular regime can be simulated using molecular dynamics (MD) or ballistic models. In the intermediate ( $0.01 < Kn < 10$ ) or rarefied regime, both collisions, with solid surfaces and with gas molecules, are important and, therefore, have to be included in the simulation to obtain an accurate result. The direct simulation Monte Carlo (DSMC) method developed by Bird [4] is the perfect practical engineering method that can be used in the rarefied regime. It is also valid in the free-molecular and continuum regimes, although computational expenses become very large in the latter case. Its computational expenses, in fact, scale with the Knudsen number and become prohibitively large when  $Kn$  becomes lower than  $\sim 0.05$ . Usually, gas flow can be simulated for  $Kn < 0.01$  using continuum-based CFD models, for  $Kn > 0.05$  using

the particle-based DSMC methods, and for  $0.05 < Kn < 0.01$  using the coupled NS/DSMC methods.

Unfortunately, hypersonic shock is not an entirely understood domain. Flow property  $\phi$  changes significantly in the inner of shock. Also, the gradient of flow property  $\partial\phi/\partial x$  is large, because characteristic dimension  $L$  is small. It causes the Knudsen number becomes big in the inner of shock. And, the Knudsen number is also big in the far field which results in the simulation difficulty of low density hypersonic flows.

In low-density hypersonic flows, both CFD and DSMC are used in the prediction of pressure and heat characteristics. However, conclusions, drawn from the simulation and experiment, are different. Unfortunately, many CFD and DSMC simulations are incompatible with precision direction [5, 6].

Some double-cone flow simulation studies, including *Candler's ect* CFD [7] and Moss DSMC simulation [8], have been conducted. In these studies, comparisons between simulation and experiment reveal significant numerical problems that can be encountered when predicting strong gradients. Experimental data are used for comparisons, as conducted in ONERA R5Ch Mach 10 low-density wind tunnel [8]. In Moss's DSMC research, VHS model was used. HS and VSS models were not included in Moss's DSMC simulation. Both in *Candler's ect* CFD [7] and in Moss's DSMC [8] research, the experimental conditions of Run numbers 26, 32, 33, 36, and 38 are not included, as shown in Table 1.

For studying the influence of the DSMC molecular model on hypersonic shock interaction, DSMC simulations are conducted by three molecular models, namely, HS [9, 10], VHS [9, 10], and VSS [11]. The simulations are focused on experimental conditions of Run numbers 26, 32, 33, 36, and 38. These conditions are not included in previous studies. For further reliability, Edney's type IV shock interaction is also studied.

## 2. DSMC Model

In DSMC, gas is represented by the velocity components and positions of a large number of simulated molecules. The position coordinates, velocity components, and internal states of the simulated molecule data are stored. These parameters are updated with time because the molecules are concurrently followed by representative collisions and boundary interactions in the simulated domain [12]. The primary approximation of DSMC is that molecular motions and intermolecular collisions are decoupled over short time intervals. The DSMC's flowchart in the current study is shown in Figure 1.

The core of the DSMC algorithm consists of four primary processes: moving the particles, indexing and cross-referencing the particles, simulating collisions, and sampling the flow field [9].

**2.1. Moving the Particles.** In the first process, all the simulated molecules are moved through distances, which are proportionate to their velocity components and discrete time

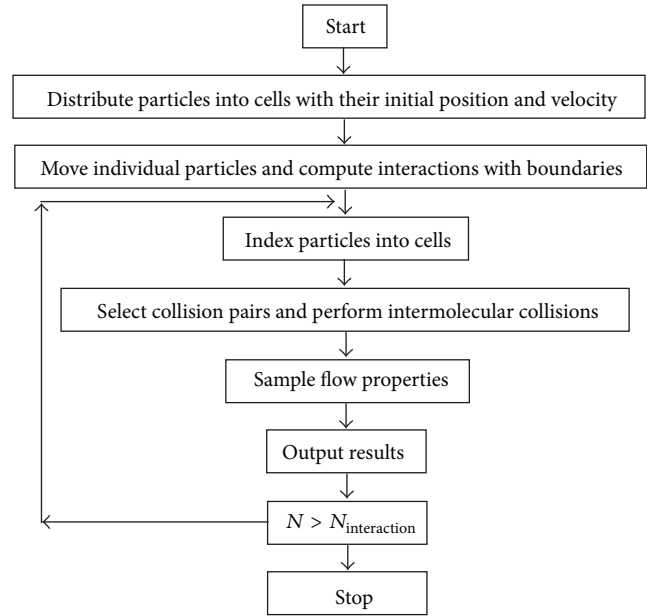


FIGURE 1: DSMC flowchart.

step. Appropriate action is taken if the molecule crosses boundaries, such as solid surfaces and symmetry boundary. Collisions with surfaces can be treated as being fully specular, fully diffuse, or any combination of the two. Specular collisions involve a simple reversal of the molecular velocity component normal to the incident surface. Diffused collisions cause a random reorientation of the reflected molecule, where the postcollision velocity is based on surface temperature.

**2.2. Indexing and Tracking the Particles.** The second DSMC process involves indexing and tracking the particles. This molecular referencing scheme is needed as prerequisite for the next two steps: modeling the collisions and sampling the flow field.

**2.3. Simulation of Collisions.** The third step, simulating collisions, is an important process. And it is different from the MD (molecular dynamics) method. In DSMC simulation, elastic collision model is used in which no interchange of translational and internal energy is considered. And also, in the collision, linear momentum and energy are conserved.

**2.3.1. Impact Parameters and Collision Cross Section.** In homogenous gas, the probability of two molecules collision is proportional to their relative speed and total collision cross section. In DSMC, cross section  $\sigma$  is defined as [13]

$$\sigma = \frac{b}{\sin \chi} \left| \frac{db}{d\chi} \right|. \quad (3)$$

Here,  $b$  is the distance of the closest approach to the undisturbed trajectories and  $\chi$  is the angle of deflection, as shown in Figure 2.

TABLE 1: Test case in [1].

Run	$V_\infty$ (m/s)	$\rho_\infty$ (Kg/m <sup>3</sup> ×10 <sup>3</sup> )	$P_\infty$ (Pa)	Ma	Re/m (×10 <sup>5</sup> )	Nose
26	2581	1.093	48.7	10.34	1.704	Sharp
28	2520	0.727	30.0	10.50	1.106	Sharp
35	2575	0.608	18.5	12.49	0.945	Sharp
32	2572	0.758	32.1	10.56	1.177	R0.250
33	2636	1.288	59.8	10.35	2.050	R0.250
36	2584	1.108	49.6	10.34	1.729	R0.250
38	2453	0.498	13.9	12.47	0.738	R0.288

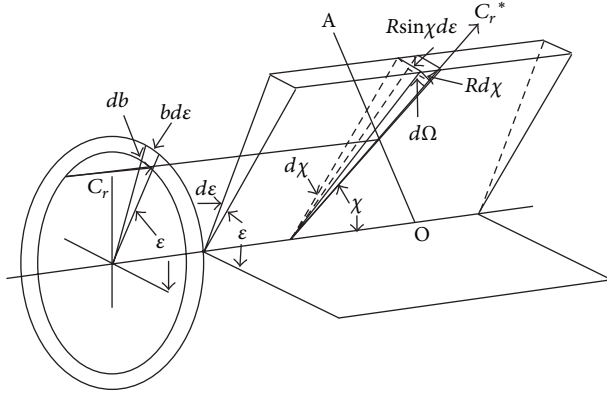


FIGURE 2: Illustration of the impact parameters [4].

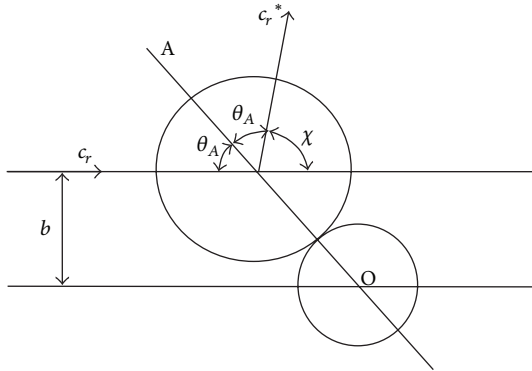


FIGURE 3: Collision geometry of HS molecules [4].

Then, the total collision cross section can be written as

$$\sigma_T = 2\pi \int_0^\pi \sigma \sin \chi d\chi = 2\pi \int b db. \quad (4)$$

Here, the distance of the closest approach  $b$  is given in different molecular model. In the current paper, three molecular models, including HS, VHS, and VSS, are used in the simulation.

(1) *HS Model*. In the HS model, the intermolecular force is effective at

$$r = \frac{1}{2} (d_1 + d_2) = d_{12}. \quad (5)$$

Then, as Shown in Figure 3, we can get the closest approach  $b$

$$b = d_{12} \cos \left( \frac{1}{2} \chi \right),$$

$$\left| \frac{db}{d\chi} \right| = \frac{1}{2} d_{12} \sin \left( \frac{1}{2} \chi \right), \quad (6)$$

$$\sigma = \frac{d_{12}^2}{4}.$$

Therefore, the total collision cross section is defined as

$$\sigma_T = \pi d_{12}^2. \quad (7)$$

In HS model, the molecule diameter can be calculated as

$$d = \left[ \frac{(5/16) (mkT_{\text{ref}}/\pi)^{1/2}}{\mu_{\text{ref}}} \right]^{1/2}, \quad (8)$$

where  $\mu_{\text{ref}}$  is the reference viscosity at temperature  $T_{\text{ref}}$  and  $m$  is the molecular mass.

$k$  is the Boltzmann constant and  $k = 1.380658 \times 10^{-23}$  J/K.

(2) *VHS Model*. In the VHS model, molecular diameter  $d$  is defined as a function of relative velocity  $C_r$ ; that is,

$$d_{\text{VHS}} = d_{\text{ref}} \left( \frac{C_{r,\text{ref}}}{C_r} \right)^\xi = \left[ \frac{(15/8) (m/\pi)^{1/2} (kT_{\text{ref}})^\omega}{\Gamma((9/2) - \omega) \mu_{\text{ref}} \epsilon_t^{\omega-(1/2)}} \right]^{1/2}. \quad (9)$$

Here,  $\mu_{\text{ref}}$  is the reference viscosity at temperature  $T_{\text{ref}}$ .  $\omega$  is the power law, which is expressed as  $\omega = (1/2) + \xi$ .  $\xi$  is relative speed exponent of VHS model and it can be adjusted to meet the power law  $\mu \propto T^\omega$ .  $\epsilon_t$  is the relative mean kinetic energy expressed as  $\epsilon_t \equiv (1/2) m_r C_r^2$ .  $C_r$  is relative speed between the collision molecules.  $C_{r,\text{ref}}$  is reference relative speed between the collision molecules.

In the VHS model, the closest approach  $b$  can be defined as

$$b = d_{\text{VHS}} \cos \left( \frac{1}{2} \chi \right). \quad (10)$$

The total collision cross section is expressed as

$$\sigma_T = \sigma_{T,\text{ref}} \left( \frac{d_{\text{VHS}}}{d_{\text{ref}}} \right)^2, \quad (11)$$

where  $\sigma_{T,\text{ref}}$  is reference collision cross section at the reference molecule diameter  $d_{\text{ref}}$ .

(3) *VSS Model*. In the VSS model, molecular diameter  $d$  is defined as

$$d_{\text{VSS}} = \left[ \frac{5(\alpha + 1)(\alpha + 2)(m/\pi)^{1/2}(kT_{\text{ref}})^{\omega}}{16\alpha\Gamma((9/2) - \omega)\mu_{\text{ref}}\epsilon_t^{\omega-(1/2)}} \right]^{1/2}. \quad (12)$$

Here,  $\alpha$  is the scattering coefficient. (In the case where  $\alpha = 1$ , the VSS model is the same as the VHS model.)

In the VSS model, the closest approach  $b$  is defined as

$$b = d_{\text{VSS}} \cos^{\alpha} \left( \frac{1}{2} \chi \right). \quad (13)$$

The total collision cross section is defined as

$$\sigma_T = \pi d_{\text{VSS}}^2. \quad (14)$$

**2.3.2. Gas-Surface Interaction.** Diffuse reflection [14] with full accommodation to the surface temperature is implemented in the simulation. It means that molecules diffused under the Maxwell distribution condition at  $T = T_W$  during the simulation.

**2.4. Sampling.** The sampling of the macroscopic flow properties is the final process in DSMC. The spatial coordinates and velocity components of the molecules in a particular cell are used to calculate the macroscopic quantities at the geometric center of the cell. Consider

$$\begin{aligned} \rho &= nm, \\ P &= \overline{\rho(c - \bar{c})^2}, \end{aligned} \quad (15)$$

where  $n$  is the number density of the molecules,  $c$  is the velocity of the molecule, and  $\bar{c}$  is the average velocity of the molecule.

**2.5. Parameters.** The parameters selected in the present paper are pressure coefficient and the Stanton number:

$$\begin{aligned} C_P &= \frac{P - P_{\infty}}{(1/2)\rho V_{\infty}^2}, \\ S_t &= \frac{q}{(1/2)\rho V_{\infty}^3}, \end{aligned} \quad (16)$$

where  $P$  is the flow-field pressure,  $P_{\infty}$  is the far-field pressure of the flow field,  $\rho$  is the density of flow-field density,  $V_{\infty}$  is the far-field velocity of the flow field, and  $q$  is the thermal flux of the solid surface.

### 3. Hypersonic Double-Cone Flow Simulation

**3.1. Moss and Boyd's DSMC Predictions for Hypersonic 25°/55° Double-Cone Flow.** To validate the DSMC method, three 25°/55° hypersonic double-cone configurations are selected under five conditions. The experimental data, with four

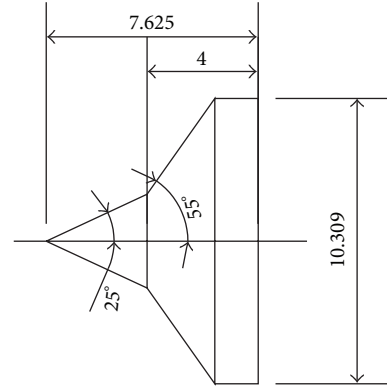


FIGURE 4: Number 1 configuration (in) (sharp nose 25°/55° double cone).

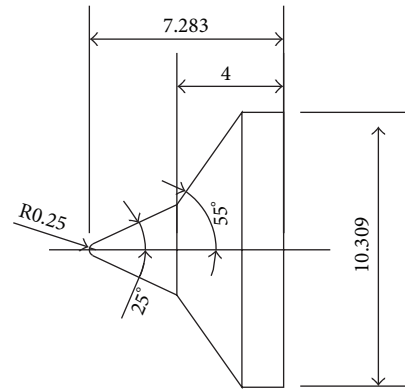


FIGURE 5: Number 2 configuration (in) (R0.25 blunt nose 25°/55° double cone).

configurations as shown in Figures 4, 5, 6, and 7 and, are reported in [1] in which Moss and Boyd's DSMC predictions are compared with the experimental data under some experimental conditions. Boyd's predictions using the DSMC code for Run number 35 are shown in Figure 8. These predictions clearly underestimated the length of the separated region, and although the heating in the forebody is slightly underpredicted, a good agreement existed between theory and experiment for the pressures and the heat transfer downstream of the shock/shock interaction in the second cone [12].

Figures 9 and 10 show the results obtained using the DSMC method by Moss [8] and Boyd [15], which significantly underpredicted the scale of the interaction region and the position and magnitude of the properties in and downstream of the region of shock/shock interaction. Moss calculations, shown in Figure 9, indicated that the predicted separated region is approximately 25% of the length measured in the experiment. Downstream of the interaction regions, the pressure and the heating levels were relatively well predicted. Boyd's solution for Run number 28 also significantly underpredicted the length of the separated region, and unlike Moss's calculation, the heat transfer rates both ahead and

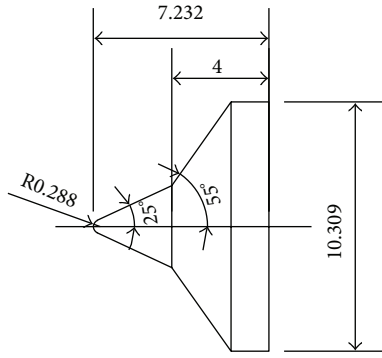


FIGURE 6: Number 3 configuration (in) (R0.288 blunt nose 25°/55° double cone).

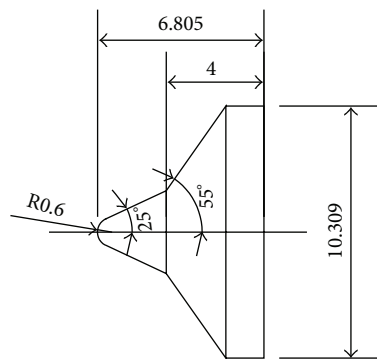


FIGURE 7: Number 4 configuration (in) (R0.6 blunt nose 25°/55° double cone).

TABLE 2: Properties of nitrogen molecule in DSMC.

Degree of freedom	5
Molecular mass $\times 10^{27}$ Kg	46.5
Viscosity coefficient	1.656
Viscosity index	0.74
$\alpha$ (for VSS model)	1.36
Molecular diameter (VHS) $\times 10^{10}$ m	4.17
Molecular diameter (VSS) $\times 10^{10}$ m	4.11
Molecular diameter (HS) $\times 10^{10}$ m	3.784

TABLE 3: Flow conditions for Run Numbers 26 and 36.

	Ma	Re/m	Kn
Run 26	10.34	$1.704 \times 10^5$	$9.05 \times 10^{-5}$
Run 36	10.34	$1.73 \times 10^5$	$8.91 \times 10^{-5}$

downstream of the interaction were underpredicted. Significant improvement of these calculations is doubtful even with the incorporation of vibrational nonequilibrium effects.

**3.2. Our DSMC Simulation.** In [1], Run numbers 26, 32, 33, 36, and 38 were not simulated by DSMC and CFD. Therefore, we selected these cases to validate the DSMC code with the HS, VHS, and VSS models.

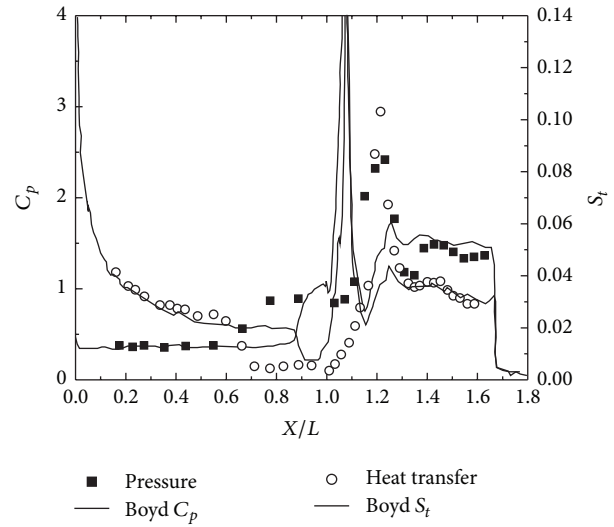


FIGURE 8: Boyd's DSMC for Run number 35 [1, 15].

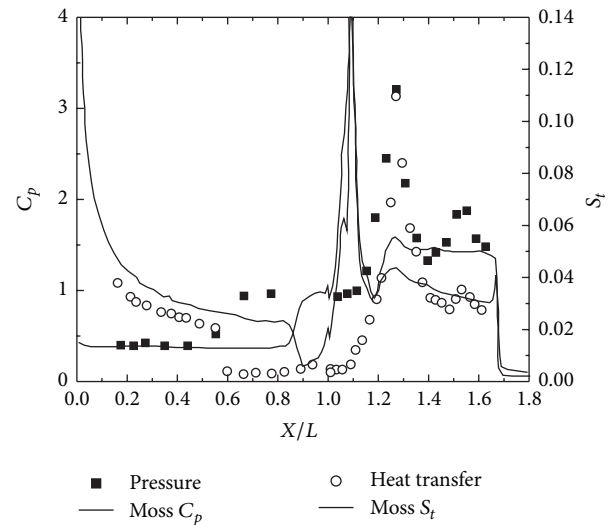


FIGURE 9: Moss's DSMC for Run number 28 [8].

The computational grid, employed for Run numbers 26, 32, 33, 36, and 38, consists of 2,048 cells along the body by 512 cells normal to the body. This grid is the same as that of Boyd's DSMC simulation [15]. The base time step for the simulation was  $10^{-9}$  s, although this was reduced in very high density regions. The solutions were obtained using approximately 6.4 million particles and averaged over a sampling interval of 0.5 ms. At this time, the solution had attained steady state. In particular, the size of the separation region did not change.

The properties of nitrogen molecule, used in the current study, are presented in Table 2.

**3.2.1. DSMC Simulation of Run Numbers 26 and 36.** In this section, the DSMC simulation result of Run numbers 26 and 36 is presented. As shown in Table 3, these two cases were conducted in the same Ma and Re conditions with sharp nose and R0.25 in blunt nose, respectively.

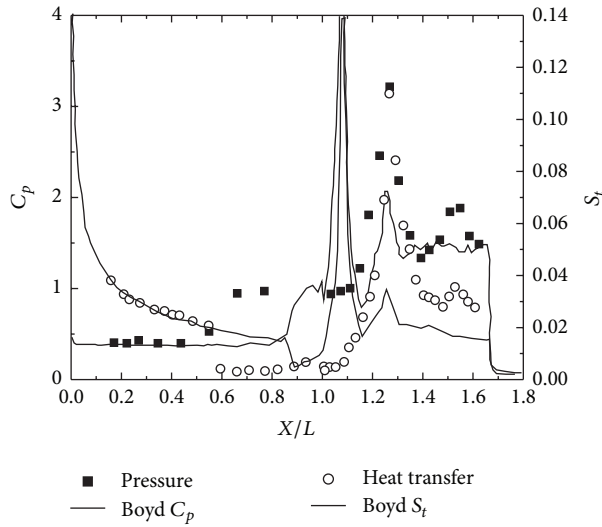
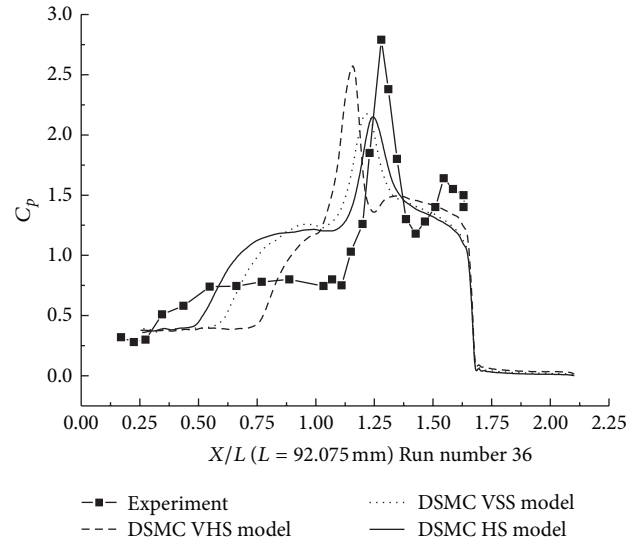
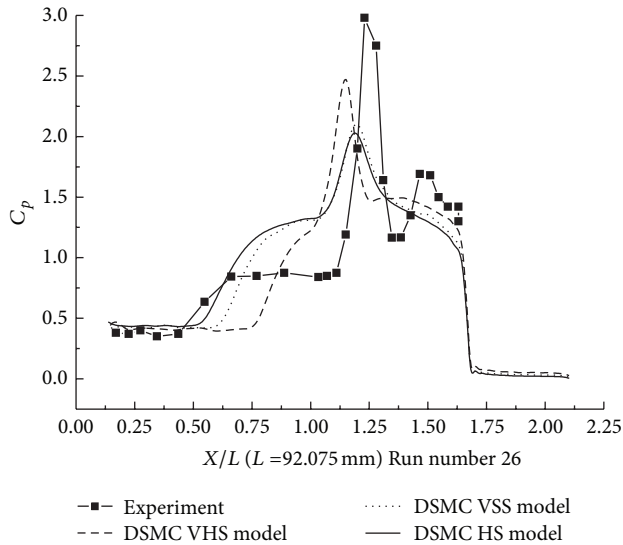
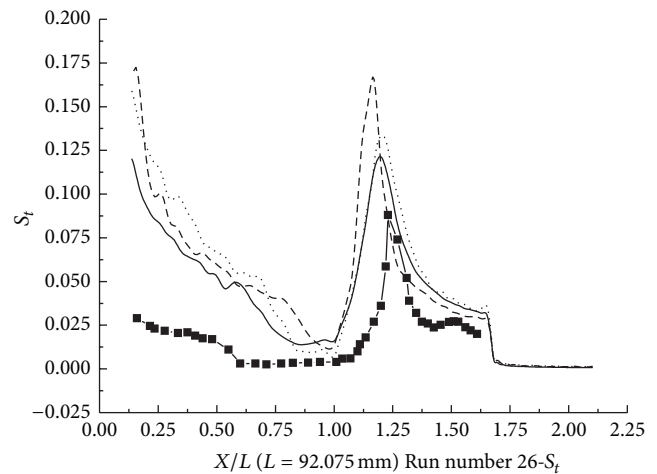


FIGURE 10: Boyd's DSMC for Run number 28 [15].

FIGURE 12: DSMC simulation of Run number 36 ( $C_p$ ).FIGURE 11: DSMC simulation of Run number 26 ( $C_p$ ).FIGURE 13: DSMC simulation of Run number 26 ( $S_t$ ).

The pressure coefficient and the Stanton number, obtained with HS, VHS, and VSS, are shown in Figures 11–14. These results underpredict the scale of interaction region and the position, and also the magnitude of the parameters is underpredicted in and downstream. The HS calculation shown in Figure 11 for Run number 26 indicates that the predicted interaction region is approximately 76% of the measured experimental length. Those of VHS and VSS are 34% and 62%, respectively. The HS results, shown in Figure 12 for Run number 36, indicate that the predicted interaction region is approximately 76% of the measured experimental length. Those of VHS and VSS are 30% and 57%, respectively. These predictions are much improved compared with Moss's DSMC calculation, which was only 25% of the length measured in the experiment [8]. The results of three models overpredicted the ahead pressure coefficient

peak value. In the downstream of the interaction regions, the pressure levels got by the three models were relatively well predicted. And also, the three models overpredicted the Stanton number in comparison with the experimental data. The position of the Stanton number peak was well predicted by the three models. Figure 13 shows that the peak values of the Stanton number using HS, VHS, and VSS are approximately 142%, 185.7%, and 148.5%, respectively, of the data measured in the experiment for Run number 26. Figure 14 shows that the peak values of the Stanton number using HS, VHS, and VSS are approximately 178%, 192.8%, and 178%, respectively, of the data measured in the experiment for Run number 36.

**3.2.2. DSMC Simulation of Run Number 33.** In this section, the DSMC simulation result of Run number 33 is presented.



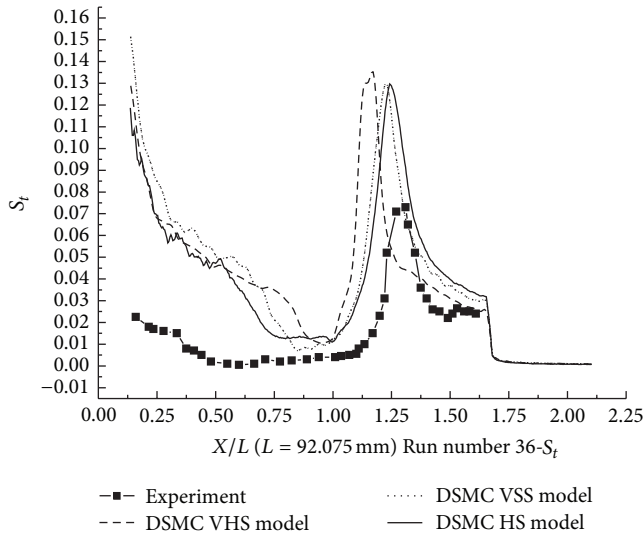
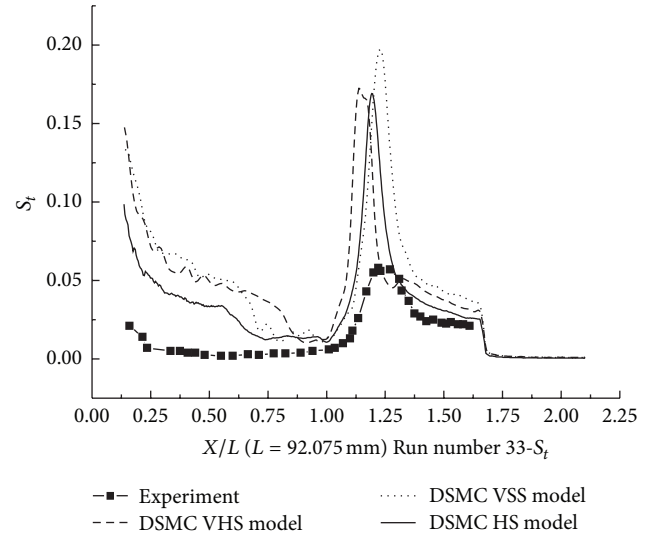
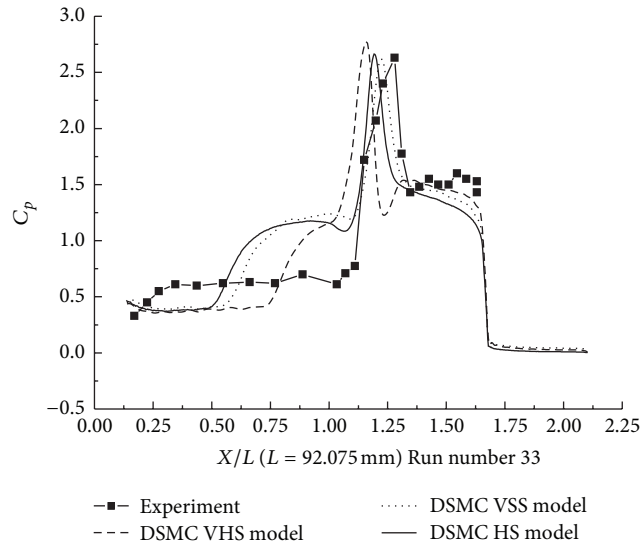
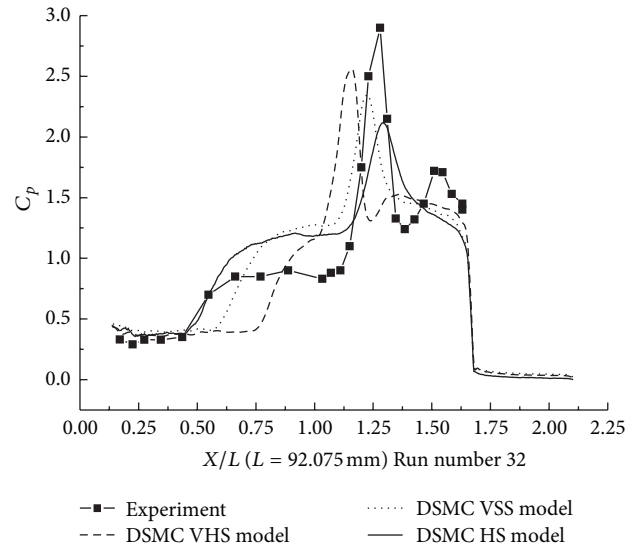
FIGURE 14: DSMC simulation of Run number 36 ( $S_t$ ).FIGURE 16: DSMC simulation of Run number 33 ( $S_t$ ).FIGURE 15: DSMC simulation of Run number 33 ( $C_p$ ).FIGURE 17: DSMC simulation of Run number 32 ( $C_p$ ).

TABLE 4: Flow conditions for Run Numbers 33 and Numbers 36.

	Ma	Re/m	Kn
Run 33	10.35	$2.05 \times 10^5$	$7.53 \times 10^{-5}$
Run 36	10.34	$1.73 \times 10^5$	$8.91 \times 10^{-5}$

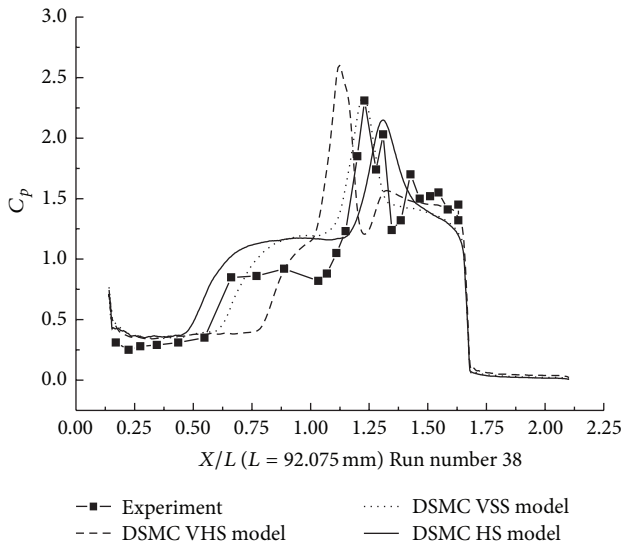
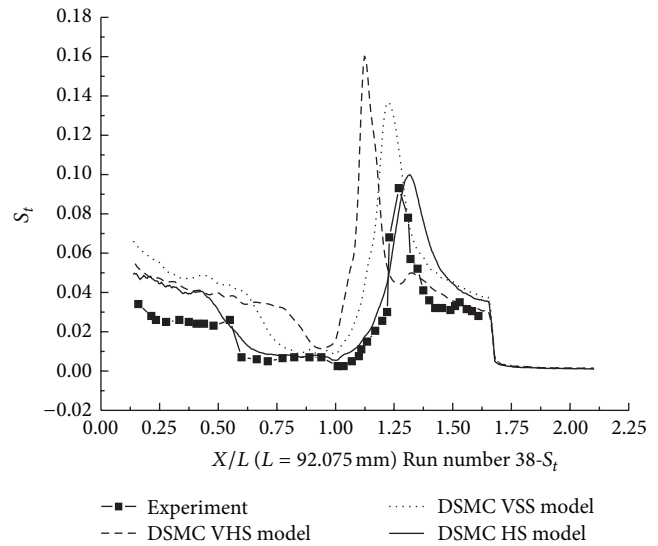
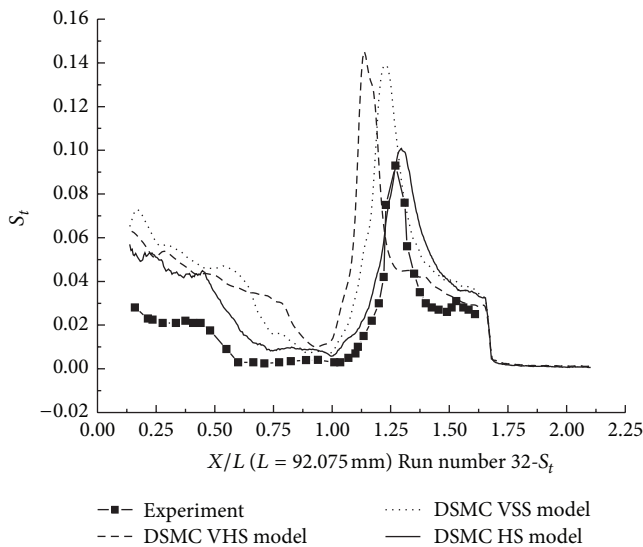
TABLE 5: Flow conditions for Run Numbers 32 and 38.

	Ma	Re/m	Kn
Run 32	10.56	$1.177 \times 10^5$	$1.34 \times 10^{-4}$
Run 38	12.47	$0.738 \times 10^5$	$2.52 \times 10^{-4}$

As shown in Table 4, Run numbers 33 and 36 were conducted in the same configuration with different Kn condition.

The pressure coefficient and the Stanton number, obtained from HS, VHS, and VSS using the DSMC

method, are shown in Figures 15 and 16. These results also underpredicted the scale of interaction region and position, magnitude of the properties in and downstream of the shock interaction region. The HS result, shown in Figure 15, indicates that the predicted interaction region is approximately 53.3% of the length measured in the experiment. Those of VHS and VSS are 26.6% and 46.6%, respectively. These predictions are not improved in comparison with Run numbers 26 and 36 calculations. The three models' calculation also overpredicted the ahead pressure coefficient peak value. In the downstream of the interaction region, the pressure levels from three models are relatively well predicted. Also, three models overpredicted the Stanton number compared with the experimental data. But, the position of the Stanton number peak is well predicted in the three models' calculation. Figure 16 shows

FIGURE 18: DSMC simulation of Run number 38 ( $C_p$ ).FIGURE 20: DSMC simulation of Run number 38 ( $S_t$ ).FIGURE 19: DSMC simulation of Run number 32 ( $S_t$ ).

that the peak values of the Stanton number in HS, VHS, and VSS are approximately 290%, 309%, and 345%, respectively, of the data measured in the experiment for Run number 33.

**3.2.3. DSMC Simulation for Run Numbers 32 and 38.** In this section, the DSMC simulation results for Run numbers 32 and 38, as shown in Table 5, are presented. Run numbers 33, 38, and 36 were conducted in the same configuration with R0.25 in blunt nose.

The pressure coefficient and the Stanton number obtained by HS, VHS, and VSS using the DSMC method are shown in Figures 17–20. These results well predicted the scale of the interaction region and the position, magnitude of the properties in and downstream of the shock interaction region. The HS result, shown in Figure 17 for Run number 32, indicates

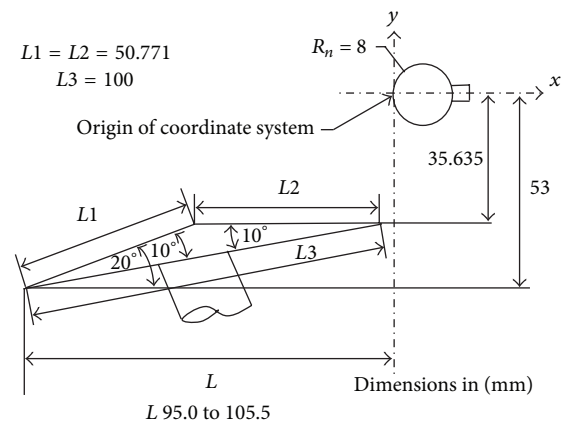
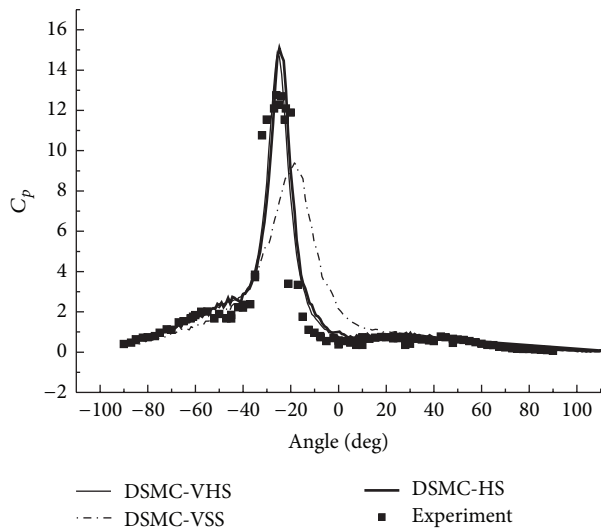
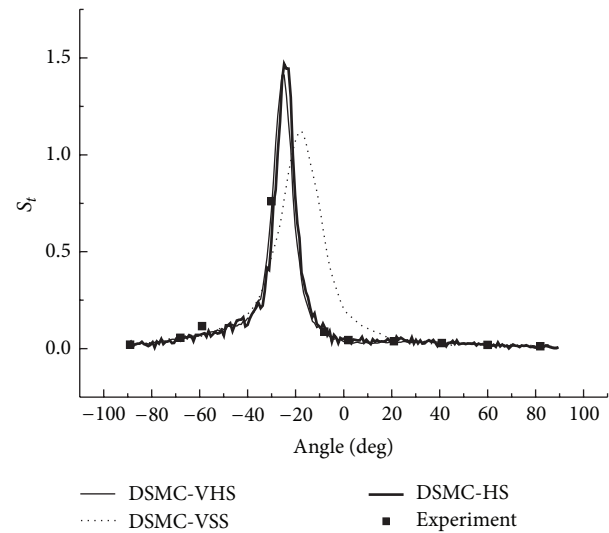


FIGURE 21: Configuration of Edney's Type IV shock interaction.

that the predicted interaction region is approximately 100% of the length measured in the experiment. Those of VHS and VSS are 41% and 69%, respectively. The HS result, shown in Figure 18 for Run number 38, indicates that the predicted interaction region is approximately 106.8% of the length measured in the experiment. Those of VHS and VSS are 27.6% and 68.96%, respectively. These predictions are improved in comparison with Run numbers 26 and 36 calculations. Also, the three models' calculation overpredicted the ahead pressure coefficient peak value. And in the downstream of interaction region, the pressure levels from the three models are relatively well predicted. The three models also overpredicted the Stanton number in comparison with the experimental data. And also, the position of the Stanton number peak is well predicted in the three models' calculation. Figure 19 shows that the peak values of the Stanton number in HS, VHS, and VSS are approximately 105.2%, 157.8%, and



FIGURE 22: DSMC of type IV shock interaction ( $C_p$ ).FIGURE 23: DSMC of type IV shock interaction ( $S_t$ ).

147.4%, respectively, of the data measured in the experiment for Run number 32. Figure 20 shows that the peak value of the Stanton number in HS, VHS, and VSS are approximately 105.2%, 168.4%, and 142.1%, respectively, of the data measured in the experiment for Run number 38.

Table 6 shows that the DSMC error depends on the Kn number and the models employed for intermolecular interaction. With the increase in the Kn number, the DSMC error decreases. The error is the smallest in the HS model compared with those in the VHS and VSS models. With the Kn number increasing, the Stanton number DSMC error decreases. When the Kn number is in the level of  $10^{-4}$ , the DSMC error for pressure coefficient and Stanton number is controlled within 10%.

#### 4. Type IV Shock Interaction Simulation

In the present study, results of the numerical simulations for Mach 10 air flow, as shown in Table 7, were presented for a range of Edney's type IV shock interaction. The experimental data for validation were obtained from [16]. The configuration is shown in Figure 21.

The results of the grid sensitivity investigation are presented in [16]. The number of cells/subcells used for our simulation was 97,060/958,490, proven in [16] to be the finest. The computational time step was 1.2 ns. The simulation consisted of  $1.56 \times 10^5$  time steps to ensure steady state conditions.

The DSMC data of the pressure coefficient and the Stanton number are shown in Figures 22 and 23. The agreement between the DSMC calculation and the experiment is generally good. Both HS and VHS models gain improvements in the errors. The error between the HS-DSMC data and the experimental data is controlled within 5%.

The result from the DSMC calculation for Edney's type IV shock interaction also confirmed the same conclusion. The

error is the smallest in the HS model compared with those in the VHS and VSS models. In the region of large Kn number, DSMC using the HS model could be used in pressure and thermal prediction of hypersonic complex flow.

#### 5. Conclusion

In the present study, the double-cone and Edney's type IV shock interactions were studied. Molecular models were employed with DSMC including the HS, VHS, and VSS models. Comparisons between DSMC and the experiment were also conducted.

Drawing firm conclusions from this study prior to full comparisons of these results is somewhat difficult. However, some issues are immediately clear from our attempt to compute these flows.

- (1) The DSMC method appears to predict qualitatively the structure of flow separation found in previous CFD calculations.
- (2) Investigation of the double-cone hypersonic flow reveals that the three collisions models can predict the pressure coefficient and the Stanton number trends. The agreement between the DSMC simulation and the experiment is the best in the HS collisions model.
- (3) Investigation of type IV shock interaction shows that the agreement between the DSMC simulation and the experiment is generally good in the HS and VHS collision models. However, it fails in the VSS model.
- (4) Both double-cone flow and type IV shock interaction simulations show that the DSMC error depends on the Kn number and the models employed for intermolecular interaction. Increasing the Kn number decreases the DSMC error. The error is the smallest for the HS model compared with those for the

TABLE 6: Comparisons of calculations  $((\text{Value}_{\text{DSMC}} - \text{Value}_{\text{experiment}})/(\text{Value}_{\text{experiment}}))$ .

Run	Kn	The scale of interaction region (error in compared with measured data %)			Peak value of the Stanton number (error in compared with measured data %)		
		HS	VHS	VSS	HS	VHS	VSS
33	$7.53 \times 10^{-5}$	46.7	73.4	53.4	190	209	245
36	$8.91 \times 10^{-5}$	24	70	43	78	92.8	78
26	$9.05 \times 10^{-5}$	24	66	38	42	85.7	48.5
32	$1.34 \times 10^{-4}$	0	59	31	5.2	57.8	47.4
38	$2.52 \times 10^{-4}$	6.8	72.4	31.04	5.2	68.4	42.1

TABLE 7: Flow conditions of Edney's type IV shock interaction.

Ma	Re/m	Kn
10	$1.03 \times 10^5$	$1.45 \times 10^{-4}$

VHS and VSS models. When the Kn number is in the level of  $10^{-4}$ , the DSMC error for pressure coefficient, the Stanton number, and scale of interaction region is controlled within 10%.

## Conflict of Interests

The authors declare that there is no conflict of interests regarding the publication of this paper.

## Acknowledgments

This work was supported in part by the Chinese Aerospace Innovation and in part by the Basic Research Fund of Northwestern Polytechnical University.

## References

- [1] M. S. Holden, T. P. Wadhams, J. K. Harvey, and G. V. Candler, "Comparisons between measurements in regions of laminar shock wave boundary layer interaction in hypersonic flows with navier-stokes and DSMC solutions," Tech. Rep. RTO-TR-AVT-007-V3, NATO Science and Technology Organization, 2006.
- [2] J. Olejniczak and G. V. Candler, "Computation of hypersonic shock interaction flow fields," in *Proceedings of the 7th AIAA/ASME Joint Thermophysics and Heat Transfer Conference*, AIAA Paper 98-2446, June 1998.
- [3] G. V. Candler, I. Nompelis, M.-C. Druguet, I. D. Boyd, W.-L. Wang, and S. M. Holden, "CFD validation for hypersonic flight: hypersonic double-cone flow simulations," in *Proceedings of the 40th Aerospace Sciences Meeting & Exhibit*, AIAA 2002-0581, Reno, Nev, USA, January 2002.
- [4] G. A. Bird, *Molecular Gas Dynamics and the Direct Simulation of Gas Flows*, Oxford Clarendon Press, New York, NY, USA, 1994.
- [5] Harvey, K. John, M. S. Holden, and T. P. Wadhams, "Code validation study of laminar shock/boundary layer and shock/shock interactions in hypersonic flow. Part B: comparison with navier-stokes and DSMC solutions," in *Proceedings of the 39th Aerospace Sciences Meeting & Exhibit*, AIAA 2001-1031, Reno, Nev, USA, January 2001.
- [6] M. Gallis, C. Roy, J. Payne, and T. Bartel, "DSMC and navier-stokes predictions for hypersonic laminar interacting flows," in *Proceedings of the 39th Aerospace Sciences Meeting and Exhibit*, AIAA 2001-1030, Reno, Nev, USA, January 2001.
- [7] G. V. Candler, I. Nompelis, and M.-C. Druguet, "Navier-stokes predictions of hypersonic double-cone and cylinder-flare flow fields," in *Proceedings of the 39th Aerospace Sciences Meeting & Exhibit*, AIAA Paper no. 2001-1024, Reno, Nev, USA, January 2001.
- [8] J. Moss, "DSMC computations for regions of shock/shock and shock/boundary layer interaction," in *Proceedings of the 39th Aerospace Sciences Meeting and Exhibit*, AIAA 2001-1027, Reno, Nev, USA, January 2001.
- [9] G. A. Bird, *The DSMC Method*, Create Space Independent Publishing Platform, 2013.
- [10] M. Woo and I. Greber, "Molecular dynamics simulation of piston-driven shock wave in hard sphere gas," *AIAA Journal*, vol. 37, no. 2, pp. 215–221, 1999.
- [11] K. Koura and H. Matsumoto, "Variable soft sphere molecular model for air species," *Physics of Fluids A*, vol. 4, no. 5, pp. 1083–1085, 1992.
- [12] P. S. Prasanth and J. K. Kakkassery, "Direct simulation Monte Carlo (DSMC): a numerical method for transition-regime flows: a review," *Journal of the Indian Institute of Science*, vol. 86, no. 3, pp. 169–192, 2006.
- [13] T. Tokumasu and Y. Matsumoto, "Dynamic molecular collision (DMC) model for rarefied gas flow simulations by the DSMC method," *Physics of Fluids*, vol. 11, no. 1, pp. 1907–1920, 1999.
- [14] S. F. Borisov, "Progress in gas-surface interaction study," in *Proceedings of the 24th International Rarefied Gas Dynamics Symposium*, M. Capitelli, Ed., pp. 933–940, The American Institute of Physics, 2005.
- [15] I. D. Boyd and W.-L. Wang, "Monte Carlo computations of hypersonic interacting flows," in *Proceedings of the 39th Aerospace Sciences Meeting and Exhibit*, AIAA Paper no. 2001-1029, Reno, Nev, USA, January 2001.
- [16] J. N. Moss, T. Pot, B. Chanetz, and M. Lefebvre, "DSMC simulation of shock/shock interactions: emphases on type IV interaction," in *Proceedings of the 22nd International Symposium on Shock Waes*, Paper no. 3570, Imperial College, London, UK, 1999.

